

Towards Accurate Multi-person Pose Estimation in the Wild

George Papandreou, Tyler Zhu, Nori Kanazawa, Alexander Toshev,
Jonathan Tompson, Chris Bregler, Kevin Murphy
Google, Inc.

[gpapan, tylerzhu, kanazawa, toshev, tompson, bregler, kpmurphy]@google.com

Abstract

We propose a method for multi-person detection and 2-D keypoint localization (human pose estimation) that achieves state-of-the-art results on the challenging COCO keypoints task. It is a simple, yet powerful, top down approach consisting of two stages.

In the first stage, we predict the location and scale of boxes which are likely to contain people; for this we use the Faster RCNN detector with an Inception-ResNet architecture. In the second stage, we estimate the keypoints of the person potentially contained in each proposed bounding box. For each keypoint type we predict dense heatmaps and offsets using a fully convolutional ResNet. To combine these outputs we introduce a novel aggregation procedure to obtain highly localized keypoint predictions. We also use a novel form of keypoint-based Non-Maximum-Suppression (NMS), instead of the cruder box-level NMS, and a novel form of keypoint-based confidence score estimation, instead of box-level scoring.

Our final system achieves average precision of 0.636 on the COCO test-dev set and the 0.628 test-standard sets, outperforming the CMU-Pose winner of the 2016 COCO keypoints challenge. Further, by using additional labeled data we obtain an even higher average precision of 0.668 on the test-dev set and 0.658 on the test-standard set, thus achieving a roughly 10% improvement over the previous best performing method on the same challenge.

1. Introduction

In the quest for comprehensive image understanding, visual interpretation of people plays a central role. We want to localize people, understand the activities they are involved in, understand how people move for the purpose of Virtual/Augmented Reality, and learn from them to teach autonomous systems. A major cornerstone in achieving these goals is the problem of human pose estimation, defined as 2-D localization of human joints on the arms, legs, and keypoints on torso and the face.

Recently, there has been significant progress on this problem, mostly by leveraging deep Convolutional Neural Networks (CNNs) trained on large labeled datasets [43, 26, 42, 10, 31, 2, 7, 6, 20, 24, 8]. However, most prior work has focused on the simpler setting of predicting the pose of a single person assuming the location and scale of the person is provided in the form of a ground truth bounding box or noisy torso keypoint, as in the popular MPII [2] and FLIC [38] datasets.

In this paper, we tackle the more challenging setting of pose detection "in the wild", in which we are not provided with the ground truth location or scale of the person instances. This is harder because it combines the problem of person detection (localization) with the problem of keypoint detection (landmarking). Furthermore, in crowded scenes, where people are close to each other, it can be quite difficult to solve the association problem of determining which body part belongs to which person.

The recently released COCO person keypoints detection dataset and associated challenge [29] provide an excellent vehicle to encourage research, establish metrics, and measure progress on this task. It extends the COCO dataset [30] with additional annotations of 17 keypoints (12 body joints and 5 face landmarks) for every medium and large sized person in each image. A large number of persons in the dataset are only partially visible. The degree of match between ground truth and predicted poses in the COCO keypoints task is measured in terms of object keypoint similarity (OKS), which ranges from 0 (poor match) to 1 (perfect match). The overall quality of the combined person detection and pose estimation system in the benchmark is measured in terms of an OKS-induced average precision (AP) metric. In this paper, we describe a system that achieves state-of-the-art results on this challenging task.

There are two broad approaches for tackling the multi-person pose estimation problem: *bottom-up*, in which keypoint proposals are grouped together into person instances, and *top-down*, in which a pose estimator is applied to the output of a bounding-box person detector. Recent work [33, 24, 8, 23] has advocated the bottom-up approach; in

their experiments, their proposed bottom-up methods outperformed the top-down baselines they compared with.

In contrast, in this work we revisit the top-down approach and show that it can be surprisingly effective. The proposed system is a two stage pipeline with state-of-art constituent components carefully adapted to our task. In the first stage, we predict the location and scale of boxes which are likely to contain people. For this we use the Faster-RCNN method [35] on top of an Inception-Resnet CNN [40]. In the second stage, we predict the locations of each keypoint for each of the proposed person boxes. For this we use a Resnet [21] applied in a fully convolutional fashion to predict activation heatmaps and offsets for each keypoint, similar to the works of Pishchulin et al. [33] and Insafutdinov et al. [24], followed by combining their predictions using a novel form of heatmap-offset aggregation. We avoid duplicate pose detections by means of a novel keypoint-based Non-Maximum-Suppression (NMS) mechanism building directly on the OKS metric (which we call OKS-NMS), instead of the cruder box-level IOU NMS. We also propose a novel keypoint-based confidence score estimator, which we show leads to greatly improved AP compared to using the Faster-RCNN box scores for ranking our final pose proposals. Our final system achieves average precision of 0.636 on the COCO test-dev set and the 0.628 test-standard sets, outperforming the winner of the 2016 COCO keypoints challenge [8], which gets 0.618 on the COCO test-dev and 0.611 on the test-standard set. Further, if we use additionally labeled data we obtain an even higher average precision of 0.668 on the test-dev set and 0.658 on the test-standard set, thus achieving a roughly 10% improvement over the next best approach on the same challenge.

In the rest of the paper, we discuss related work, and then describe our method in more detail. We then perform an experimental study, comparing our system to recent state-of-the-art, and we measure the effects of the different parts of our system on the AP metric.

2. Related Work

For most of its history, the research in human pose estimation has been heavily based on the idea of part-based models, as pioneered by the Pictorial Structures model of Fischer and Elschlager [16]. One of the first practical and well performing methods based on this idea is Deformable Part Model (DPM) by Felzenswalb et al. [15], which spurred a large body of work on probabilistic graphical models (PGM) for 2-D human pose inference [3, 12, 37, 45, 11, 27, 32, 38, 18]. The majority of these methods focus on developing tractable inference procedures for highly articulated models, while at the same time capturing rich dependencies among body parts and properties.

Single-Person Pose With the development of Deep Convolutional Neural Networks (CNN) for vision tasks, state-

of-art performance on pose estimation is achieved using CNNs [43, 26, 42, 10, 31, 2, 7, 6, 20, 24, 8]. The problem can be encoded as simple regression, as done by Toshev and Szegedy [43], using a cascade of detectors for top-down pose refinement from cropped input patches. Alternatively, Jain et al. [26] trained a CNN on image patches, which was applied convolutionally at inference time to infer heatmaps (or activity-maps) for each keypoint independently. In addition, they used a “DPM-like” graphical-model post processing step to filter heatmap potentials and to impose inter-joint consistency. Following this work, Tompson et al. [42] used a multi-scale fully-convolutional architecture trained on whole images (rather than image crops) to infer the heatmap potentials, and they reformulated the graphical model from [26] - simplifying the tree structure to a star-graph and re-writing the belief propagation messages - so that the entire system could be trained end-to-end.

Chen et al. [10] added image-dependant priors to improve CNN performance. By learning a lower-dimensional image representation, they clustered the input image into a mixture of configurations of each pair of consecutive joints. Depending on which mixture is active for a given input image, a separate pairwise displacement prior was used for graphical model inference, resulting in stronger pairwise priors and improved overall performance.

Bulat et al. [7] use a cascaded network to explicitly infer part relationships to improve inter-joint consistency, which the authors claim effectively encodes part constraints and inter-joint context. Similarly, Belagiannis & Zisserman [6] also propose a cascaded architecture to infer pairwise joint (or part) locations, which is then used to iteratively refine unary joint predictions, where unlike [7], they propose iterative refinement using a recursive neural network.

Inspired by recent work in sequence-to-sequence modeling, Gkioxari et al. [20] propose a novel network structure where body part locations are predicted sequentially rather than independently, as per traditional feed-forward networks. Body part locations are conditioned on the input image and all other predicted parts, yielding a model which promotes sequential reasoning and learns complex inter-joint relationships.

The state-of-the-art approach for single-person pose on the MPII human pose [2] and FLIC [38] datasets is the CNN model of Newell et al. [31]. They propose a novel CNN architecture that uses skip-connections to promote multi-scale feature learning, as well as a repeated pooling-upsampling (“hourglass”) structure that results in improved iterative pose refinement. They claim that their network is able to more efficiently learn various spatial relationship associated with the body, even over large pixel displacements, and with a small number of total network parameters.

Top-Down Multi-Person Pose The problem of multi-person pose estimation presents different challenges, un-

addressed by the above work. Most of the approaches for multi-person pose aim at associating human part detections with human instances. The *top down* way to establish these associations, which is closest to our approach, is to first perform person detection followed by pose estimation. For example, Pishchulin et al. [34] follow this paradigm by using PS-based pose estimation. A more robust to occlusions person detector, modelled after poselets, is used by Gkioxari et al. [19]. Further, Yang and Ramanan [45] fuse detection and pose in one model by using a PS model. The inference procedure allows for pose estimation of multiple instance in one image analogous to PS-based object detection. A similar multi-person PS with an additional explicit occlusion modeling is proposed by Eichner and Ferrari [13].

On a related note, 2-D person detection is used as a first step in several 3D pose estimation works [39, 4, 5].

Bottom-Up Multi-Person Pose A different line of work is to detect body parts instead of full persons, and to subsequently associate these parts to human instances, thus performing pose estimation in a *bottom up* fashion. Such approaches employ part detectors and differ in how associations among parts are expressed, and the inference procedure used to obtain full part groupings into person instances. Pishchulin et al. [33] and later Insafutdinov et al. [24, 23] formulate the problem of pose estimation as part grouping and labeling via a Linear Program. A similar formulation is proposed by Iqbal et al. [25].

A probabilistic approach to part grouping and labeling is proposed also by Ladickly et al. [28]. The authors model human part to human instance associations in addition to pixel-wise human and human part segmentation. They leverage a HOG-based system for part detections.

Cao et al. [8] obtained state-of-the-art results on the 2016 COCO person keypoints challenge [30] by combining a variation of the unary joint detector architecture from [44] with a part affinity field regression to enforce inter-joint consistency. They propose a greedy algorithm to generate person instance proposals in a bottom-up fashion. Their best results are obtained in an additional top-down refinement process in which they run a standard single-person pose estimator [44] on the person instance box proposals generated by the bottom-up stage.

3. Methods

Our multi-person pose estimation system is a two step cascade, as illustrated in Figure 1. In the first stage, we use a person detector to produce a bounding box around each person instance. In the second stage, we apply a pose estimator to the image crop extracted around each detected person instance in order to localize its keypoints.

Our approach is inspired by recent state-of-art object detection systems such as [17, 41], which propose objects in a class agnostic fashion as a first stage and refine their la-

bel and location in a second stage. We can think of the first stage of our method as a proposal mechanism, however of only one type of object – person. Our second stage serves as a refinement where we (i) go beyond bounding boxes and predict keypoints and (ii) rescore the detection based on the estimated keypoints. For computational efficiency, we only forward to the second stage person box detection proposals with score higher than 0.3, resulting in only 3.5 proposals per image on average. In the following, we describe in more detail the two stages of our system.

3.1. Person Box Detection

Our person detector is a Faster-RCNN system [35], with the important modification that we use ResNet-Inception architecture [40]. This architecture combines Inception layers [41] with residual connections [21] and performs better than both of its components. The detector is initially trained on all 80 categories in the COCO dataset. It is further modified so it only predicts the location of one class – ‘person’. We fine-tune the modified model on data which contains only person bounding boxes. Our system is based on the Faster-RCNN implementation of [22].

To achieve even better performance, we also consider a variant in which the person detector is an ensemble of two Faster-RCNN models, one based on [40] as described above, and one based on ResNet [21] for higher model diversity. To combine these, we first run the region proposal net for both models, and then apply the box refinement and scoring nets for both models on all proposals. We further improve performance by applying the ensembled detector to the whole image, as well as to 9 crops, arranged in a 3x3 grid; this helps detect small people. We discuss the improvements obtained by these extensions in Section 4.

3.2. Person Pose Estimation

The pose estimation component of our system predicts the location of all $K = 17$ person keypoints, given each person bounding box proposal delivered by the first stage.

One approach would be to use a single regressor per keypoint, as in [43], but this is problematic when there is more than one person in the image patch (in which case a keypoint can occur in multiple places). A different approach addressing this issue would be to predict activation maps, as in [26], which allow for multiple predictions of the same keypoint. However, the size of the activation maps, and thus the localization precision, is limited by the size of the net’s output feature maps, which is a fraction of the input image size, due to the use of max-pooling with decimation.

In order to address the above limitations, we adopt a combined classification and regression approach. For each spatial position, we first classify whether it is in the vicinity of each of the K keypoints or not (which we call a “heatmap”), then predict a 2-D local offset vector to get a

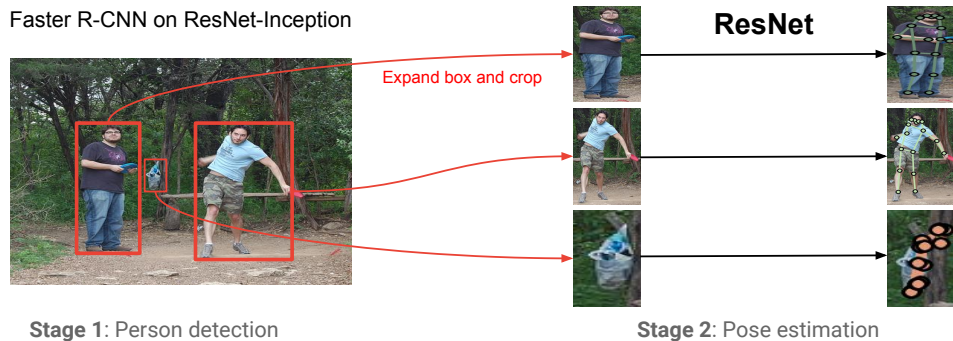


Figure 1: Overview of our two stage cascade model.

more precise estimate of the corresponding keypoint location. Note that this approach is inspired by work on object detection, where a similar setup is used to predict bounding boxes, e.g. [14, 35]. Figure 2 illustrates these three output channels per keypoint.

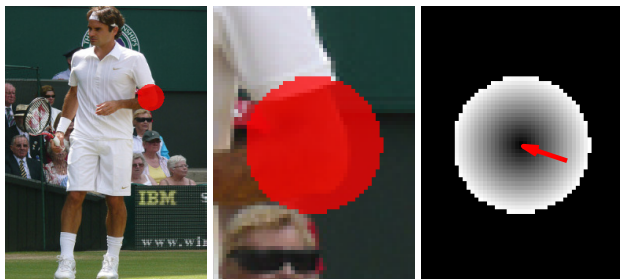


Figure 2: Network input and ground-truth outputs. *Left & Middle:* left-elbow heatmap overlay (red indicates heatmap of 1). *Right:* offset L2 magnitude (2-D offset vector shown in red).

Image Cropping We first make all boxes have the same fixed aspect ratio (height / width = 1.37) by extending either the height or the width of the boxes returned by the person detector without distorting the image aspect ratio. After that, we further enlarge the boxes to include additional image context: we use a rescaling factor equal to 1.25 during evaluation and a random rescaling factor between 1.0 and 1.5 during training (for data augmentation). We then crop from the resulting box the image and resize to a fixed crop of height 353 and width 257 pixels.

Heatmap and Offset Prediction with CNN We apply a ResNet with 101 layers [21] on the cropped image in a fully convolutional fashion to produce heatmaps (one channel per keypoint) and offsets (two channels per keypoint for the x- and y- directions), for a total of $3K$ output channels. We initialize our model from the publicly available Imagenet

pretrained ResNet-101 model of [21], replacing its last layer with 1×1 convolution with $3K$ outputs. We follow the approach of [9]: we employ atrous convolution to generate the $3K$ predictions with an output stride of 8 pixels and bilinearly upsample them to the 353×257 crop size.

In more detail, given the image crop, let $f_k(x_i) = 1$ if the k -th keypoint is located at position x_i and 0 otherwise. Here $k \in \{1, \dots, K\}$ is indexing the keypoint type and $i \in \{1, \dots, N\}$ is indexing the pixel locations on the 353×257 image crop grid. Training a CNN to produce directly the highly localized activations f_k (ideally delta functions) on a fine resolution spatial grid is hard.

Instead, we decompose the problem into two stages. First, for each position x_i and each keypoint k , we compute the probability $h_k(x_i) = 1$ if $\|x_i - l_k\| \leq R$ that the point x_i is within a disk of radius R from the location l_k of the k -th keypoint. We generate K such heatmaps, solving a binary classification problem for each position and keypoint independently.

In addition to the heatmaps, we also predict at each position i and each keypoint k the 2-D offset vector $F_k(x_i) = l_k - x_i$ from the pixel to the corresponding keypoint. We generate K such vector fields, solving a 2-D regression problem for each position and keypoint independently.

After generating the heatmaps and offsets, we aggregate them to produce highly localized activation maps $f_k(x_i)$ as follows:

$$f_k(x_i) = \sum_j \frac{1}{\pi R^2} G(x_j + F_k(x_j) - x_i) h_k(x_j), \quad (1)$$

where $G(\cdot)$ is the bilinear interpolation kernel. This is a form of voting process: each point j in the image crop grid casts a vote with its estimate for the position of every keypoint, with the vote being weighted by the probability that it is in the disk of influence of the corresponding keypoint. The normalizing factor equals the area of the disk and ensures that if the heatmaps and offsets were perfect, then

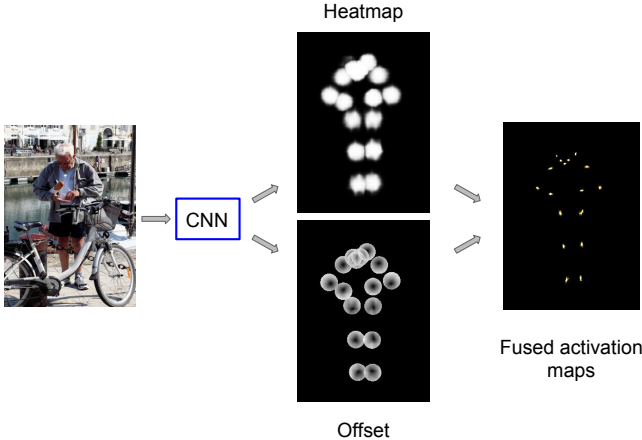


Figure 3: Our fully convolutional network predicts two targets: (1) Disk-shaped heatmaps around each keypoint and (2) magnitude of the offset fields towards the exact keypoint position within the disk. Aggregating them in a weighted voting process results in highly localized activation maps. The figure shows the heatmaps and the pointwise magnitude of the offset field on a validation image. Note that in this illustration we super-impose the channels from the different keypoints.

$f_k(x_i)$ would be a unit-mass delta function centered at the position of the k -th keypoint.

The process is illustrated in Figure 3. We see that predicting separate heatmap and offset channels and fusing them by the proposed voting process results into highly localized activation maps which precisely pinpoint the position of the keypoints.

Model Training We use a single ResNet model with two convolutional output heads. The output of the first head passes through a sigmoid function to yield the heatmap probabilities $h_k(x_i)$ for each position x_i and each keypoint k . The training target $\bar{h}_k(x_i)$ is a map of zeros and ones, with $\bar{h}_k(x_i) = 1$ if $\|x_i - l_k\| \leq R$ and 0 otherwise. The corresponding loss function $L_h(\theta)$ is the sum of logistic losses for each position and keypoint separately. To accelerate training, we follow [24] and add an extra heatmap prediction layer at intermediate layer 50 of ResNet, which contributes a corresponding auxiliary loss term.

For training the offset regression head, we penalize the difference between the predicted and ground truth offsets. The corresponding loss is

$$L_o(\theta) = \sum_{k=1:K} \sum_{i: \|l_k - x_i\| \leq R} H(\|F_k(x_i) - (l_k - x_i)\|), \quad (2)$$

where $H(u)$ is the Huber robust loss, l_k is the position of the k -th keypoint, and we only compute the loss for positions x_i within a disk of radius R from each keypoint [35].

The final loss function has the form

$$L(\theta) = \lambda_h L_h(\theta) + \lambda_o L_o(\theta), \quad (3)$$

where $\lambda_h = 4$ and $\lambda_o = 1$ is a scalar factor to balance the loss function terms. We sum this loss over all the images in a minibatch, and then apply stochastic gradient descent.

An important consideration in model training is how to treat cases where multiple people exist in the image crop in the computation of heatmap loss. When computing the heatmap loss at the intermediate layer, we exclude contributions from within the disks around the keypoints of background people. When computing the heatmap loss at the final layer, we treat as positives only the disks around the keypoints of the foreground person and as negatives everything else, forcing the model to predict correctly the keypoints of the person in the center of the box.

Pose Rescoring At test time, we apply the model to each image crop. Rather than just relying on the confidence from the person detector, we compute a refined confidence estimate, which takes into account the confidence of each keypoint. In particular, we maximize over locations and average over keypoints, yielding our final instance-level pose detection score:

$$\text{score}(\mathcal{I}) = \frac{1}{K} \sum_{k=1}^K \max_{x_i} f_k(x_i) \quad (4)$$

We have found that ranking our system’s pose estimation proposals using 4 significantly improves AP compared to using the score delivered by the Faster-RCNN box detector.

4. Experimental Evaluation

4.1. Experimental Setup

The person detection and pose inference models from Sections 3.1 and 3.2 respectively, are implemented in Tensorflow [1]. We use distributed training across several machines equipped with Tesla K40 GPUs. For the person detector training we use 9 GPUs. We optimize with SGD with momentum (momentum is set to 0.9). The starting learning rate is 0.001 and is decreased by one factor every 400000 steps. We stop training after 1.5 million steps, which happens after approximately 3 days. For fine tuning on person data we use the same setup, however we usually train for less than 1 million steps.

For the pose estimator we use the same optimizer with the same optimization parameters and a batch size of 24. Training converges after 800000 steps which corresponds to one day of training.

All our networks are pre-trained on the Imagenet classification dataset [36]. To fine-tune our pose network we use

two dataset variants; one that uses only external data (*ext-only*), and one that appends to this dataset samples from an internal dataset (*int+ext*). For the *ext-only* dataset we combine training samples from the MPII human pose [2] (24,987 images with 40,614 person instances) and MS COCO pose challenge [30] (45,174 images with 105,698 person instances) datasets. Our *int+ext* dataset appends an additional 73,024 images randomly selected from Flickr, with 227,029 person instances labeled using an annotation strategy similar to that described by Lin et al. [29]. These additional training samples are verified to have no overlap with the MS COCO training, validation or test sets.

Our pose-detector model is based on the ResNet-101 [21] image classification architecture. ResNet is a very deep neural network, which contains residual connections leading to state of art performance on a variety of vision tasks [21]. We present results of this pose network trained on both the *ext-only* and *int+ext* dataset variants.

We present results using two person-detector architectures as detailed in Section 3.1: one comprised of an expensive ensemble of person-detector networks, with a multi-crop and multi-scale sampling strategy (*ensemble* model), and one that uses a significantly more efficient single-model detector network, with single-crop sampling (*single* model). We train both the person-detector model variants (*ensemble* and *single* models) on the COCO detection dataset only (our *ext-only* set without MPII samples).

4.2. COCO Keypoints Detection State-of-the-Art

Table 1 shows the COCO keypoint test-dev split performance of our two model and two dataset variants, resulting in 4 experiments in total; our pose detector trained on *ext-only* and *int+ext* datasets, as well as the *ensemble* and *single* person-detector networks. A random selection of test-dev inference samples are shown in Figure 4 (using the *ensemble* person-detector and *int+ext* pose-detector networks).

Table 2 shows the COCO keypoint test-standard split results of our *ensemble* person-detector model with pose-detector trained on both dataset variants (*ext-only* and *int+ext*).

All our model and dataset variants achieve state-of-the-art results on the MS COCO test-dev and test-standard split. Our best model uses the expensive *ensemble* person-detector trained on *ext-only* data and our pose-detector trained on *int+ext* data, for an AP score of 0.668 on test-dev. Using *ext-only* data for both models we achieve 0.636 on test-dev. The previous test-dev state-of-the-art is 0.618 from the CMU-Pose team [8].

4.3. OKS-based non maximum suppression

Following standard practice, we use non maximal suppression (NMS) to eliminate multiple detections in the person-detector stage. The standard approach measures

Table 3: Performance (AP) on COCO test-dev: with and without our proposed OKS-based NMS, using *ext-only* and *int+ext* data and the *ensemble* person-detector.

NMS Threshold	AP: <i>ext-only</i> data	AP: <i>int+ext</i> data
0.1	0.615	0.646
0.2	0.63	0.663
0.3	0.634	0.668
0.4	0.636	0.668
0.5	0.635	0.667
0.6	0.635	0.667
0.7	0.632	0.666
0.8	0.626	0.659
0.9	0.617	0.65
No NMS	0.601	0.628

overlap using intersection over union (IoU) of the boxes. We propose a more refined variant, that takes the keypoints into account. In particular, we measure the OKS score between corresponding keypoints for two candidate detections, and average this over all keypoints. We then use this as a measure of multiple detections. Applying this OKS-based NMS works well when we adjust the person detector candidate box threshold to bias towards false positives. If we aggressively suppress candidates from the person-detector, the final OKS score is lower. We attribute this to the pose network’s improved ability to reason about the person instance score as a sum of keypoint likelihood scores, and so false positives from the person-detector can be easily removed if no keypoints are present in the bounding-box, or if there is significant overlap in the joint annotations of spurious person detections.

We evaluate our proposed NMS algorithm using our *ensemble* person-detector, on both *ext-only* and *int+ext* datasets, and with multiple NMS threshold values. The results are shown in Table 3. Using *ext-only* data, NMS improves AP by 0.035 at a threshold of 0.4, which alone beats the previously reported state-of-the-art on MS COCO. Using *int+ext* data, NMS results in a significant 0.04 AP improvement.

4.4. Multi-scale Experiments

An important hyper-parameter in our cascaded system a scaling factor, s , which determines the cropped image context for input to our pose detector network. Empirically, we find a strong trade-off between pose detector input resolution and context, where too little resolution leads to inadequate high-frequency textural information, while too little context makes inferring body geometry difficult. During evaluation, we artificially enlarge the person-detector network’s bounding-box instances by scale factor s , which introduces additional image context around the subject of interest. The resultant image crop is then re-scaled to a fixed resolution of 353x257 before input to the pose detector network. Table 4 shows our cascaded detector’s AP perfor-

Table 1: Performance on COCO keypoint **test-dev** split.

	AP	AP .5	AP .75	AP (M)	AP (L)	AR	AR .5	AR .75	AR (M)	AR (L)
CMU-Pose [8]:	0.618	0.849	0.675	0.571	0.682	0.665	0.872	0.718	0.606	0.746
This work: <i>ext-only & ensemble</i>	0.636	0.852	0.7	0.596	0.702	0.685	0.881	0.741	0.635	0.754
This work: <i>ext-only & single</i>	0.624	0.840	0.685	0.591	0.681	0.667	0.866	0.720	0.608	0.749
This work: <i>int+ext & ensemble</i>	0.668	0.863	0.734	0.630	0.733	0.716	0.896	0.776	0.669	0.782
This work: <i>int+ext & single</i>	0.661	0.860	0.729	0.63	0.715	0.703	0.881	0.762	0.647	0.781

Table 2: Performance on COCO keypoint **test-standard** split.

	AP	AP .5	AP .75	AP (M)	AP (L)	AR	AR .5	AR .75	AR (M)	AR (L)
CMU-Pose[8]:	0.611	0.844	0.667	0.558	0.684	0.665	0.872	0.718	0.602	0.749
This work: <i>ext-only & ensemble</i>	0.628	0.840	0.689	0.599	0.682	0.685	0.880	0.741	0.631	0.758
This work: <i>int+ext & ensemble</i>	0.658	0.851	0.723	0.629	0.713	0.717	0.895	0.778	0.662	0.792

Table 4: Performance on COCO test-dev: varying pose detector scale. Using *single* network person detection.

scale factor (s)	AP: <i>int+ext</i> data
1.00	0.635
1.25	0.663
1.50	0.657
1.75	0.635

mance when varying scale parameter, s .

Table 4 shows that person scale and detector context play a important role in AP performance. Given a cropped input, where a single subject is centered in the middle of the cropped context, the pose network must learn an inference model that “chooses” the joints of the correct subject. With too little or too much context, this task is made difficult. In addition, increasing s in our formulation increases context at the expense of input resolution, which can also negatively effect AP performance when the crop scale is too high.

5. Conclusion

In this work we address the problem of person detection and pose estimation in cluttered images in the wild. We present a simple two stage system, consisting of a person detection stage followed by a keypoint estimation stage for each person. Despite its simplicity it achieves state-of-art results as measured on the challenging COCO benchmark.

In the future, we plan to investigate systems, that share features between the detector and keypoint estimation and can be trained end-to-end. In this way we could hopefully boost our performance further while reducing computation at inference time.

Acknowledgments

We are grateful to the authors of [22] for making their excellent Faster-RCNN implementation available to us. We would like to thank Hartwig Adam for supporting this project at its various stages, as well as Akshay Gogia and

Gursheesh Kour for managing our internal image annotation effort.

References

- [1] M. Abadi, A. Agarwal, P. Barham, E. Brevdo, Z. Chen, C. Citro, G. S. Corrado, A. Davis, J. Dean, M. Devin, S. Ghemawat, I. Goodfellow, A. Harp, G. Irving, M. Isard, Y. Jia, R. Jozefowicz, L. Kaiser, M. Kudlur, J. Levenberg, D. Mané, R. Monga, S. Moore, D. Murray, C. Olah, M. Schuster, J. Shlens, B. Steiner, I. Sutskever, K. Talwar, P. Tucker, V. Vanhoucke, V. Vasudevan, F. Viégas, O. Vinyals, P. Warden, M. Wattenberg, M. Wicke, Y. Yu, and X. Zheng. TensorFlow: Large-scale machine learning on heterogeneous systems, 2015. Software available from tensorflow.org. 5
- [2] M. Andriluka, L. Pishchulin, P. Gehler, and B. Schiele. 2d human pose estimation: New benchmark and state of the art analysis. In *CVPR*, 2014. 1, 2, 7, 10
- [3] M. Andriluka, S. Roth, and B. Schiele. Pictorial structures revisited: People detection and articulated pose estimation. In *CVPR*, 2009. 2
- [4] V. Belagiannis, S. Amin, M. Andriluka, B. Schiele, N. Navab, and S. Ilic. 3d pictorial structures for multiple human pose estimation. In *CVPR*, pages 1669–1676, 2014. 3
- [5] V. Belagiannis, S. Amin, M. Andriluka, B. Schiele, N. Navab, and S. Ilic. 3d pictorial structures revisited: Multiple human pose estimation. In *CVPR*, 2015. 3
- [6] V. Belagiannis and A. Zisserman. Recurrent human pose estimation. In *arxiv*, 2016. 1, 2
- [7] A. Bulat and G. Tzimiropoulos. Human pose estimation via convolutional part heatmap regression. In *ECCV*, 2016. 1, 2
- [8] Z. Cao, T. Simon, S.-E. Wei, and Y. Sheikh. Realtime multi-person 2d pose estimation using part affinity fields. *arXiv:1611.08050*, 2016. 1, 2, 3, 7, 8
- [9] L.-C. Chen, G. Papandreou, I. Kokkinos, K. Murphy, and A. L. Yuille. Deeplab: Semantic image segmentation with deep convolutional nets, atrous convolution, and fully connected crfs. *arXiv:1606.00915*, 2016. 4
- [10] X. Chen and A. Yuille. Articulated pose estimation by a graphical model with image dependent pairwise relations. In *NIPS*, 2014. 1, 2

- [11] M. Dantone, J. Gall, C. Leistner, and L. V. Gool. Human pose estimation using body parts dependent joint regressors. In *CVPR*, 2013. 2
- [12] M. Eichner and V. Ferrari. Better appearance models for pictorial structures. In *BMVC*, 2009. 2
- [13] M. Eichner and V. Ferrari. We are family: Joint pose estimation of multiple persons. In *ECCV*, pages 228–242. Springer, 2010. 3
- [14] D. Erhan, C. Szegedy, A. Toshev, and D. Anguelov. Scalable object detection using deep neural networks. In *CVPR*, pages 2147–2154, 2014. 4
- [15] P. Felzenszwalb, D. McAllester, and D. Ramanan. A discriminatively trained, multiscale, deformable part model. In *CVPR*, 2008. 2
- [16] M. A. Fischler and R. Elschlager. The representation and matching of pictorial structures. In *IEEE TOC*, 1973. 2
- [17] R. Girshick, J. Donahue, T. Darrell, and J. Malik. Rich feature hierarchies for accurate object detection and semantic segmentation. In *CVPR*, pages 580–587, 2014. 3
- [18] G. Gkioxari, P. Arbelaez, L. Bourdev, and J. Malik. Articulated pose estimation using discriminative armlet classifiers. In *CVPR*, 2013. 2
- [19] G. Gkioxari, B. Hariharan, R. Girshick, and J. Malik. Using k-poselets for detecting people and localizing their keypoints. In *CVPR*, pages 3582–3589, 2014. 3
- [20] G. Gkioxari, A. Toshev, and N. Jaitly. Chained predictions using convolutional neural networks. In *ECCV*, 2016. 1, 2
- [21] K. He, X. Zhang, S. Ren, and J. Sun. Deep residual learning for image recognition. In *CVPR*, 2016. 2, 3, 4, 7
- [22] J. Huang, V. Rathod, C. Sun, M. Zhu, A. Korattikara, A. Fathi, I. Fischer, Z. Wojna, Y. Song, S. Guadarrama, et al. Speed/accuracy trade-offs for modern convolutional object detectors. *arXiv:1611.10012*, 2016. 3, 8
- [23] E. Insafutdinov, M. Andriluka, L. Pishchulin, S. Tang, B. Andres, and B. Schiele. Articulated multi-person tracking in the wild. *arXiv:1612.01465*, 2016. 1, 3
- [24] E. Insafutdinov, L. Pishchulin, B. Andres, M. Andriluka, and B. Schiele. Deepcut: A deeper, stronger, and faster multi-person pose estimation model. In *ECCV*, 2016. 1, 2, 3, 5, 10
- [25] U. Iqbal and J. Gall. Multi-person pose estimation with local joint-to-person associations. In *ECCV*, pages 627–642. Springer, 2016. 3
- [26] A. Jain, J. Tompson, M. Andriluka, G. Taylor, and C. Bregler. Learning human pose estimation features with convolutional networks. In *ICLR*, 2014. 1, 2, 3
- [27] S. Johnson and M. Everingham. Learning Effective Human Pose Estimation from Inaccurate Annotation. In *CVPR*, 2011. 2
- [28] L. Ladicky, P. H. Torr, and A. Zisserman. Human pose estimation using a joint pixel-wise and part-wise formulation. In *CVPR*, pages 3578–3585, 2013. 3
- [29] T.-Y. Lin, Y. Cui, G. Patterson, M. R. Ronchi, L. Bourdev, R. Girshick, and P. Dollr. Coco 2016 keypoint challenge. 2016. 1, 7
- [30] T.-Y. Lin, M. Maire, S. Belongie, J. Hays, P. Perona, D. Ramanan, P. Dollár, and C. L. Zitnick. Microsoft coco: Common objects in context. In *ECCV*, pages 740–755. Springer, 2014. 1, 3, 7
- [31] A. Newell, K. Yang, and J. Deng. Stacked hourglass networks for human pose estimation. In *ECCV*, 2016. 1, 2, 10
- [32] L. Pishchulin, M. Andriluka, P. Gehler, and B. Schiele. Poselet conditioned pictorial structures. In *CVPR*, 2013. 2
- [33] L. Pishchulin, E. Insafutdinov, S. Tang, B. Andres, M. Andriluka, P. Gehler, and B. Schiele. Deepcut: Joint subset partition and labeling for multi person pose estimation. In *CVPR*, 2016. 1, 2, 3
- [34] L. Pishchulin, A. Jain, M. Andriluka, T. Thormählen, and B. Schiele. Articulated people detection and pose estimation: Reshaping the future. In *CVPR*, pages 3178–3185, 2012. 3
- [35] S. Ren, K. He, R. Girshick, and J. Sun. Faster R-CNN: Towards Real-Time object detection with region proposal networks. In *NIPS*, 2015. 2, 3, 4, 5
- [36] O. Russakovsky, J. Deng, H. Su, J. Krause, S. Satheesh, S. Ma, Z. Huang, A. Karpathy, A. Khosla, M. Bernstein, A. C. Berg, and L. Fei-Fei. ImageNet Large Scale Visual Recognition Challenge. *IJCV*, 115(3):211–252, 2015. 5
- [37] B. Sapp, C. Jordan, and B. Taskar. Adaptive pose priors for pictorial structures. In *CVPR*, 2010. 2
- [38] B. Sapp and B. Taskar. Modec: Multimodal decomposable models for human pose estimation. In *CVPR*, 2013. 1, 2
- [39] M. Sun and S. Savarese. Articulated part-based model for joint object detection and pose estimation. In *ICCV*, pages 723–730, 2011. 3
- [40] C. Szegedy, S. Ioffe, and V. Vanhoucke. Inception-v4, inception-resnet and the impact of residual connections on learning. *arXiv:1602.07261*, 2016. 2, 3
- [41] C. Szegedy, W. Liu, Y. Jia, P. Sermanet, S. Reed, D. Anguelov, D. Erhan, V. Vanhoucke, and A. Rabinovich. Going deeper with convolutions. In *CVPR*, pages 1–9, 2015. 3
- [42] J. Tompson, A. Jain, Y. LeCun, and C. Bregler. Joint training of a convolutional network and a graphical model for human pose estimation. In *NIPS*, 2014. 1, 2
- [43] A. Toshev and C. Szegedy. Deeppose: Human pose estimation via deep neural networks. In *CVPR*, 2014. 1, 2, 3
- [44] S.-E. Wei, V. Ramakrishna, T. Kanade, and Y. Sheikh. Convolutional pose machines. In *arXiv*, 2016. 3
- [45] Y. Yang and D. Ramanan. Articulated pose estimation with flexible mixtures of parts. In *CVPR*, 2011. 2, 3

Supplementary Experiments

Pose Given Ground Truth Person Boxes

In order to identify how many errors in our system’s output are due to using an imperfect person box detector, we conducted an experiment to measure the performance of our system given ground truth bounding boxes on a small mini-val set of 4,301 images held out from the COCO 2014 validation set (which was not used in training either the box person detector or the pose estimator). In Table 5 we compare the performance of our system using our best pose estimator trained on both *int+ext* in conjunction with either our best *single* person-detector or with the ground truth boxes supplied by the dataset. We see that using ground truth boxes increases the performance of our system in terms of AP from 0.681 to 0.720, showing that future progress in person box detection can lead to significantly improved results in our multi-person pose estimation setting.

Table 5: Performance on COCO keypoint **mini-val**: Using detected (*int+ext* & *single* model) vs. ground truth boxes.

	AP	AP .5	AP .75	AP (M)	AP (L)	AR	AR .5	AR .75	AR (M)	AR (L)
Detected boxes	0.681	0.854	0.744	0.645	0.743	0.720	0.877	0.778	0.663	0.800
Ground-truth boxes	0.720	0.905	0.792	0.699	0.760	0.751	0.919	0.813	0.711	0.809

Effect of Box Scaling Factor

Table 6 expands Table 4 of the main paper, giving the full range of AP and AR results on COCO test-dev when varying the value of the box scaling factor s from 1.00 to 1.75 during evaluation.

Table 6: Performance on COCO **test-dev**, using *single* network person detector and pose estimator trained on *int+ext* data: Varying the box scaling factor.

scale factor (s)	AP	AP .5	AP .75	AP (M)	AP (L)	AR	AR .5	AR .75	AR (M)	AR (L)
1.00	0.635	0.846	0.694	0.598	0.696	0.680	0.872	0.731	0.623	0.757
1.25	0.663	0.865	0.728	0.636	0.714	0.709	0.890	0.768	0.656	0.782
1.50	0.657	0.865	0.728	0.637	0.702	0.704	0.890	0.768	0.653	0.776
1.75	0.635	0.856	0.711	0.623	0.670	0.684	0.884	0.751	0.635	0.753

Performance on MPII Single Person Pose Estimation Task

We have also evaluated the performance of our pose estimation module alone on the standard single-person MPII human pose estimation dataset [2]. We have divided the training part of the dataset into a *MPII-train* split (14,464 images with 23,167 person instances) and a *MPII-val* split (3,612 images with 5,716 person instances). Training only on this MPII-train split yields a PCKh@0.5 performance of 89.0% on MPII-val. This is comparable to the 88.5% number reported by [24], which uses a ResNet-101 pose estimation network backbone similar to ours. Pretraining on the COCO keypoints data and fine-tuning on MPII-train improves PCKh@0.50 on MPII-val to 91.3%. Pretraining on both the COCO keypoints and our internal pose data and fine-tuning on MPII-train further improves PCKh@0.50 on MPII-val to 92.0%. The previous best reported PCKh@0.50 number on MPII is 90.9%, achieved by [31] using only MPII training data. Our results are summarized in Table 7.

Table 7: Performance of our pose estimation module on the single-person task, measured on MPII-val: Effect of additional training data.

training data	PCKh@0.50
MPII	89.0
MPII + COCO	91.3
MPII + COCO + internal	92.0